Chapter 7

Isotropic 2-D modelling

7.1 The ocean effect

Before the modelling of field data is presented, the strong induction effect observed at coasts that are close to the deep sea is considered here. This phenomenon, which is based on the enormous land–sea conductivity contrast, is well known and has been repeatedly investigated theoretically (*Fischer* [1979]; *Fischer and Weaver* [1986]; with a more realistic model: *Berdichevsky and Zhdanov* [1984], p. 130). Sea water conductivity depends mainly on salinity and temperature and ranges from above 5 S/m close to the surface to below 3.5 S/m below the main thermocline (*Horne and Frysinger* [1963]), and will thus exceed typical continental conductivities by a factor of $\gtrsim$1000.

A simple 2-D model was constructed to illustrate the spatial variation of the magnetic field around the land–sea interface, especially onshore (figure 7.1). The model besides bathymetry also includes a very fine discretized onshore topography, both adjusted to the setting in northern Chile. For simplicity, subsurface, resp. 'subsea' resistivity is homogenous with $100\,\Omega$m, and the ocean's resistivity, as in all following sections of this work, is set to $0.27\,\Omega$m. Calculations were performed with the finite element code from *Wannamaker et al.* [1987]. Offshore data are responses on the water surface.

Figure 7.1 shows the transfer functions z_D and d_D, i.e. the anomalous vertical and horizontal magnetic field, both referred to the horizontal field at a reference situated $340\,$km away from the coast in the eastern 'Altiplano', for the periods $100\,$s and $3300\,$s. Since the horizontal anomalous field is enhanced above concentration of horizontal currents ($\Re[d_D] > 0$) and decreased above zones of current dilution ($\Re[d_D] < 0$), a qualitative current distribution is best estimated by interpreting the transfer function d_D. At short periods ($100\,$s), anomalous oceanic currents concentrate above the continental slope, and towards longer periods they spread out seawards, even beyond the deep ocean trench. Current densities onshore are decreased at all periods, which is reflected in a negative anomalous horizontal magnetic field there ($\Re[d_D] < 0$ — in magnetotellurics, this is reflected in very low apparent resistivities in the TE-polarization, see *Fischer and Weaver* [1986]). Due to the offshore current concentration, the vertical magnetic field is positive downward on land ($\Re[z_D] > 0$). The longer the period, the farer inland the ocean effect is observed. Note that the spatial gradient of d_D onshore is very small, which is also observed in the geomagnetic field data from both study areas.
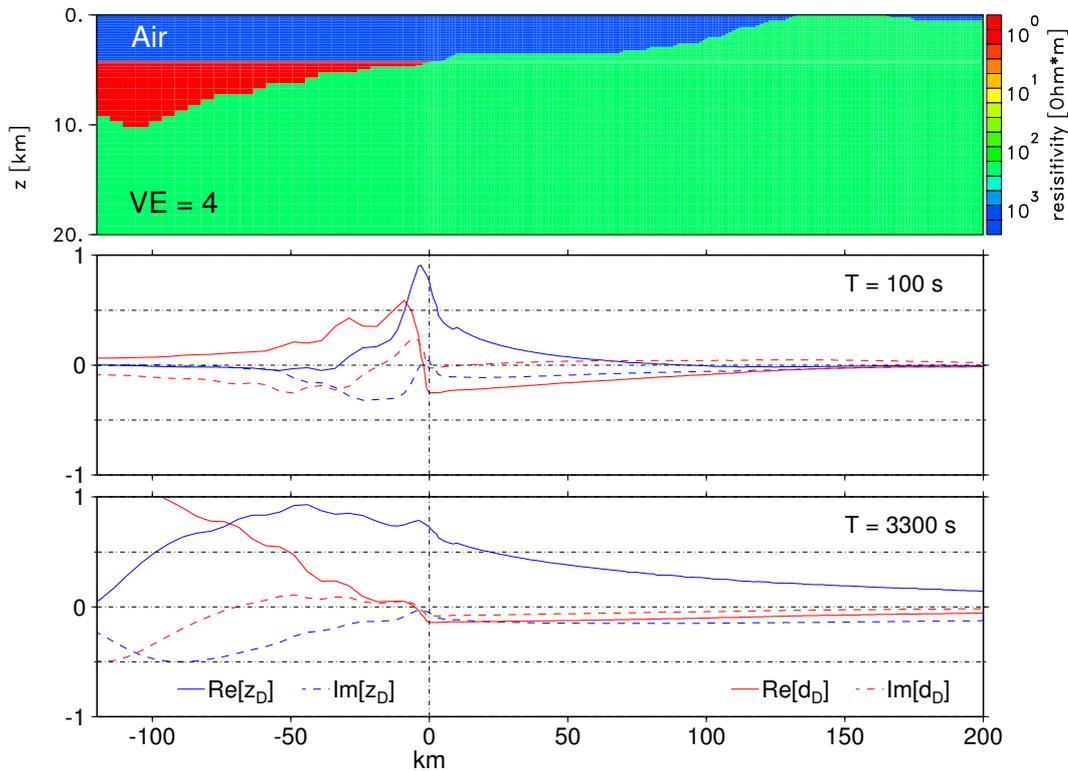
Figure 7.1: A simple model simulating electromagnetic induction at a land–sea border, deduced from the setting in northern Chile. Responses $z_D = B_z/B_{y0}$ and $d_D = (B_y - B_{y0})/B_{y0}$ for periods 100 s and 3300 s are shown in the plots below. Reference for B_{y0} is chosen 340 km inland, which corresponds to the eastern Altiplano.

In addition to the investigation of the coast effect, this modelling also reveals that for a homogenous subsurface, the relative difference of elevation between the Longitudinal Valley and the Precordillera ($\sim$4000 m) has no inductive response for the period range considered.

7.2 On the sensitivity and accuracy of the two polarizations

Though for ideal data sets which are continuous in time/frequency and space and noise-free, the magnetotelluric and geomagnetic transfer functions above a 2-D subsurface all contain full information on the subsurface conductivity distribution (section 6.1.2), the synthetic modelling presented in section 6.4 clearly shows that the two polarization modes, respectively their responses, have very different sensitivities to specific structures of the conductivity model. From the inversion results of both models, it can be concluded that the TM-mode is insensitive to small-scale conductive features that are embedded in a resistive host and do not reach the surface. The TE-mode, in contrast, is particularly sensitive to these structures. On the other hand, responses of the TM-polarization well reflect the 1-D background distribution of the model of figure 6.1, whereas in the TE-polarization, the lower part of it is masked by the inductive response of the conductive features above.

Berdichevsky et al. [1998] demonstrated at a model simulating an uprise of a conductive asthenosphere into the resistive lithosphere, that the TE-polarization is also more sensitive to deep-seated conductive anomalies, whereas in this example the TM-polarization is more sensitive to the resistivity of the lithosphere above. In presence of small superficial conductivity anomalies, due to the quasi-static effect of surface charge accumulation, apparent resistivities in the TM-polarization towards longer periods are shifted by a constant factor, whereas the TE-mode is not affected, since here currents flow parallel to conductivity contrasts (cf. equation 2.31, for synthetic examples see also *Berdichevsky et al.* [1998]).

The sensitivity of responses to certain structures of the model, which are here considered as deviations from a 1-D distribution, is directly related to anomalous currents caused by these structures. Thus, physically the geomagnetic transfer functions of the TE-mode are sensitive to the same structures as are magnetotelluric data of this mode, although for expanded and/or more complicated structures, this generalization must be revised (see numerical examples from section 6.4).

Now we consider 3-D conductivity distributions which still have a preferred strike direction, so that the two polarizations can be referred to as *longitudinal* (currents along 'strike') and *transverse*. The confined along 'strike' extent of conductive anomalies strongly influences all transfer functions related to the longitudinal polarization, but since now quasi-static effects do also occur in this mode, apparent resistivities are especially impaired by the lateral limiting. *Wannamaker et al.* [1984] studied this effect for a 'prismatic sedimentary-basin model', an elongated superficial good conductor embedded in an upper resistive layer of a one-dimensional background, comparing the 3-D responses with the respective two-dimensional responses. Whereas both, apparent resistivities and phases of the transverse polarization are totally insensitive to the lateral extent, magnetotelluric responses of the longitudinal polarization differ strongly: apparent resistivities above and aside the anomaly are shifted downwards, and, only above the anomaly, also phases are much higher. In contrast, the principal signature in the local geomagnetic transfer function remains, but the maximum is decreased and shifted towards shorter periods, and values decrease with increasing distance from the contrast more rapidly.

Berdichevsky et al. [1998] extended this study, constructing a model that simulates a confined elongated region of a reduced, compared to the surrounding area very thin sedimentary cover above a resistive crust, thus comprising a resistive superficial anomaly. Now, aside the anomaly, instead of current gathering, the structure provokes a current around flow in the transverse polarization, decreasing current densities and thus shifting *down* apparent resistivities with respect to the 2-D response, while the longitudinal polarization is almost unaltered. *Berdichevsky et al.* [1998] conclude: "The TM impedance is more robust to 3-D effects caused by conductive structures (that is, by current gathering), but the TE impedance may be more robust to 3-D effects caused by resistive structures."[1] Still, as mentioned, the sensitivity of the TE impedances to 3-D effects caused by conductive structures is much higher than that of the geomagnetic data of the same polarization.

---

[1] This obvious complementary is just one aspect of a more general 'principle of complementary in magnetotellurics' in this context, that is derived in *Berdichevsky et al.* [1998].

In the examinations on the robustness of the impedances to superficial 3-D effects cited above, the background conductivity distribution was always one-dimensional. In a 2-D background, the accuracy of the 2-D approximation of the two modes additionally depends on the regional fields: in section 5.1 it is shown that in the area affected by the coast effect, the impedance of the longitudinal polarization is extremely sensitive to any superficial 3-D effects, whereas in the geomagnetic transfer functions of the same polarization, the effect of scatterers is minute.

For cases where also deep structures are of finite extent and/or the preferred strike direction of deep and superficial structures differ, it is useful to invert different data types separately when approaching to the physical content of the data, particularly if the main strike direction is supposed to be known. For such environments it may be questioned, if it is reasonable to present and discuss one final model. Finally, also the synthetic examples of section 6.4 illustrate that even for true 2-D data an inversion of single data types gives different, resp. complementary information on the conductivity distribution.

7.3   Central Andes

Before any 2-D modelling, usually dimensionality analysis of the MT impedance tensor together with an inspection of the local induction vectors is performed. In this study, also geomagnetic perturbation matrices can be taken into account to investigate the feasibility of a 2-D approach. Investigation on the effect of local 3-D scatterers at stations which are strongly affected by the coast effect showed that magnetic transfer functions related to an inducing *magnetic* longitudinal polarization (h_H, d_H, z_H, T_x) are strongly affected by the scattering, whereas those related to an inducing magnetic transverse polarization (h_D, d_D, z_D, T_y) are as robust to distortion as is the impedance phase of the electric transverse mode (see section 5.1). Thus, any tensor rotations following the Swift-equivalent approach of *Siemon* [1991] (equation 2.27) would contaminate the information contained in the transfer functions T_y, d_D and z_D. Therefore, dimensionality analysis based on geomagnetic transfer functions besides the investigation in section 5.1 has been omitted.[2]

Data for this study were intensively investigated by *Echternacht et al.* [1997], *Lezaeta* [2001], *Schwalenberg* [2000] and *Brasse et al.* [2002]. Most (recent) dimensionality analysis was done by *Lezaeta* [2001], who's thesis essentially bases on the circumstance that the data are not truly two-dimensional. Strong current channelling is proposed there to account for highly distorted field data in the Coastal Cordillera, including both, telluric and magnetic quasi-static distortion. This is in very good agreement with the observed geomagnetic perturbations. Since at these stations, impedance phases of the electric longitudinal polarization run out of quadrant, they can not be included in the modelling. To not omit these data completely in the modelling, for stations PEN, GLO, LAY, CDL and PDT impedances Z_{xy} and Z_{yx} were replaced by the respective eigenvalues resulting from an eigenstate analysis after *Eggers* [1982] (see also *Lezaeta* [2001]). In the Precordillera, observed 3-D effects do not fit the current channelling model and are thus supposed to be of inductive nature.[3] Yet, also on

---

[2]A phase sensitive skew of the perturbation matrix, equivalent to that for the impedance tensor (*Bahr* [1988]) might be a better means to quantify quasi-static magnetic distortion, as proposed by *Leibecker* [2000]. However, this has not been tested.

[3]In both, data and modelling, the Precordillera anomaly is stronger in the north, which also points at
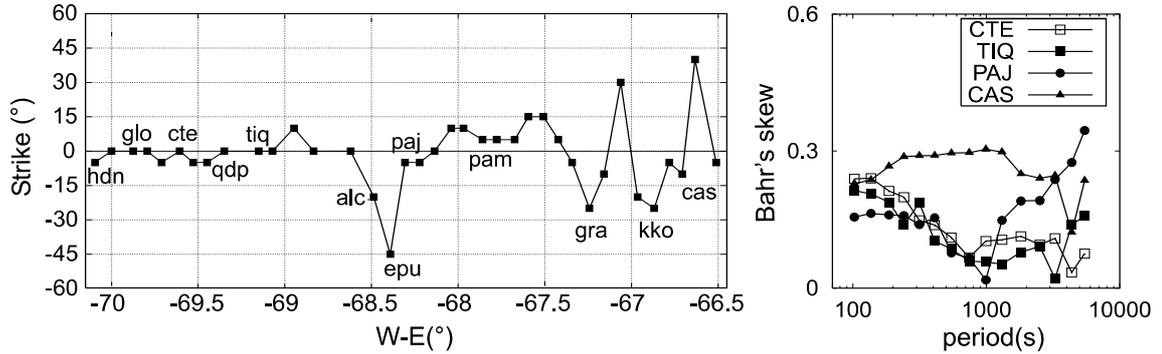
Figure 7.2: Left: period averaged (1000s – 6000s) regional strike direction for the ANCORP profile, calculated from an analysis after Groom and Bailey [1989] (from Brasse et al. [2002]). Right: Regional skew values after Bahr [1988] for representative stations from four geological units (P. Lezaeta, pers. comm.).

account of the coast effect, for both regions the strike direction for the ANCORP profile is approximately N-S (figure 7.2). In the Western Cordillera and in the eastern Altiplano the regional strike directions deviate markedly from E-W direction. The phase sensitive skew, in figure 7.2 shown for four representative sites, on the eastern Altiplano is close to the 'tolerable' empiric threshold of 0.3, indicating three-dimensionality. For the data along the PICA profile, *Echternacht et al.* [1997] deduced a strike direction of N-8°W.

After all, the data are obviously not too three-dimensional for any 2-D investigation, and *Schwalenberg* [2000] performed joint 2-D inversions of unrotated apparent resistivities and phases, employing the finite differences code from *Rodi and Mackie* [2001], using the Gauß-Newton method for the inversion procedure. To account for quasi-static distortion effects, apparent resistivities were downweighted with respect to the phases. This is of particular importance for data of the longitudinal (TE) polarization, since in the transverse polarization, the inversion procedure can reproduce static effects by inclusion of small-scale superficial heterogeneities, which merely do impair the results for deeper seated structures if strong shift is not observed at too many sites. With other words, only for the TM-mode, static shift is contained in the physics of 2-D electromagnetic induction. The resulting model of this study is presented and described in section 3.1.

Various investigations were performed within this modelling to test for the model structures. Amongst others, these are: the influence of the Lagrange-multiplier and of the model roughness operator (first/second differences) on the the inversion results, inclusion of structures in the start, resp. a priori model ($\mathbf{m}_0$), investigation of the sensitivity matrix, some forward modelling studies and inversion of data from a subset of stations (the latter did not have much influence on the results). Though the overall fit of the inverted data by the final model response is rather good (RMS = 3.44), local geomagnetic transfer functions, which could not be incorporated in the inversion procedure, are not fit within this modelling: the signature of the Precordillera anomaly in the data is much stronger than in the model response, and towards longer periods the location of zero B_z variation ($T_y = 0$), for isolated symmetric structures marking the center of the anomaly, is strongly shifted westward in the response.

---

three-dimensionality (cf. figures 5.4 and 3.5).
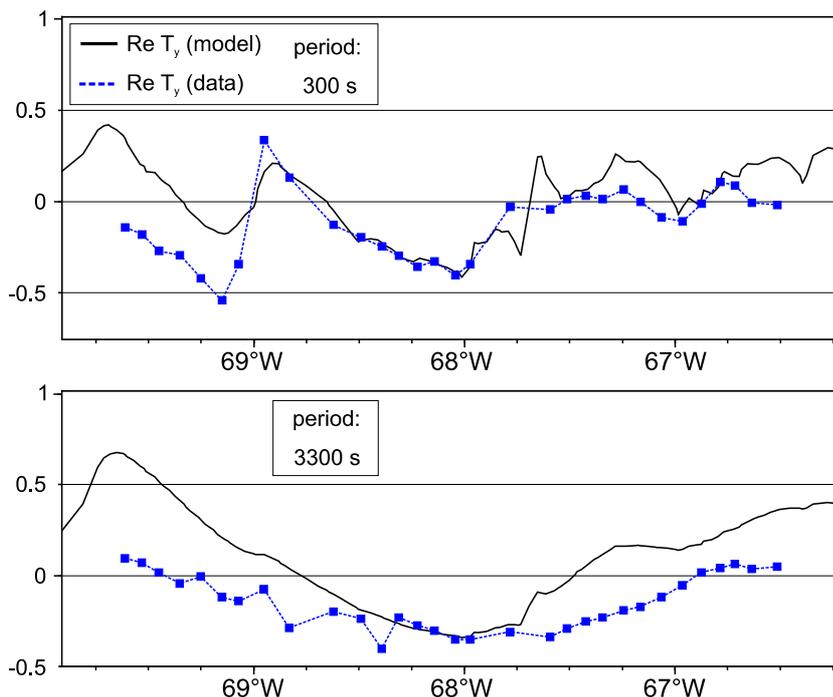
Figure 7.3: East component of local tipper function for 300 s and 3300 s along the ANCORP line (CTE-CAS): data (dashed line) and model response (solid) of the favored model from Schwalenberg [2000] (forward calculation with the code from Rodi and Mackie [2001]).

The ocean was not included as a priori structure in the start, resp. a priori model. Still, in the inversion yielding the model presented in *Brasse et al.* [2002] the ocean was included, and both models are very similar.

In this work, since three more data types are available, the 2-D investigation aims at getting insights in the subsurface conductivity distribution by examining the information contained in the different types of transfer functions: apparent resistivities and phases of both polarizations, local geomagnetic transfer functions T_y, and the inter-station geomagnetic transfer functions d_D (horizontal to horizontal) and z_D (vertical to horizontal).

Section 4.3 documented, how the separately processed arrays consisting of 3 to 6 field sites were successively combined to one final synthetic array following the scheme sketched in figure 4.4. From this resulting array, arbitrary inter-station of local transfer functions can be calculated. In figures 5.4 & 5.5 from section 5.1 data from the synthetic array were presented, whereby all fields within the array were related to the horizontal magnetic field of station CTE, located in the Longitudinal Valley. Spatially, the results were consistent suggesting also high quality of these data. Yet, unfortunately the successive combination leads to contamination of good data due to comparably bad data from the overlapping stations of the first campaign in 1993 (mainly EPU and CRU), which is immediately recognized when plotting data from Bolivia as a function of period. Also, the for the combination necessary assumption that the horizontal magnetic fields at stations EPU and PAJ are equal has to be rejected for a full quantitative investigation, additionally since the error of such assumption

would impair all data from the Bolivian part of the study area. Therefore, data from this synthetic array have only been analyzed by a 'qualitative' 2-D modelling, which is presented in *Soyer and Brasse* [2001].

To deal with the best available data — transfer functions directly calculated from the output of the multivariate processing — is was decided to invert for data with various but as few references as reasonable, and combination of arrays has mostly been avoided. This has also the advantage that data from more stations can be included in the inversion procedure: one sub-array from the Chile 1993 campaign including site HUA which is directly located above the Precordillera anomaly. The finally chosen site – reference site combination grouping is illustrated in table 7.1.

Site	HDN	PEN	GLO	LAY	CDL	CTE	PDT	KOZ	QDP	CCO
Ref.	CTE	CTE	CTE	CTE	CTE	ALC	CTE	CCO	CTE	KOZ

Site	TIQ	HUA	COC	QBA	CAR	ALC	EPU	PAJ	HIU	MOP
Ref.	CTE	KOZ	CTE	EPU	CTE	CAR	QBA	VAD	VAD	VAD

Site	TAR	LUX	PAM	CHU	PAY	JUL	KHA	KHU	MAN	GRA
Ref.	VAD	PAJ	PAJ	HIU	PAJ	PAJ	PAJ	VAD	JUL	JUL

Site	YAN	VAD	RAM	KKO	CAL	MIK	VIL	CAS
Ref.	PAJ	CAS	PAJ	VAD	MAN	KHA	VAD	VAD

Table 7.1: Site – reference site organization for the horizontal to horizontal, resp. vertical to horizontal inter-station transfer functions d_D and z_D.

Figure 7.4 presents results from separate inversions of the five available data types for the ANCORP profile. All calculations were performed with the REBOCC inversion code, extended as documented in section 6. The models comprise 200 columns and 50 rows (plus 10 air layers for the TE-mode), and the Pacific ocean was included in the start resp. a priori model, which was fixed during the inversions as an extremely low resistive structure of realistic $0.27\,\Omega$m, its lower bound roughly tracing the true bathymetry with a ~ 7 km deep trench. Apart from the ocean, the two models are homogeneous with a resistivity of $1000\,\Omega$m. Note that with REBOCC, the earth's surface can only be modelled flat without accounting for topography. As representer basis for the calculation of the sensitivity matrix, a subset of every second period at all stations was chosen (see section 6.2 and *Siripunvaraporn and Egbert* [2000] for explanation). Error floors in the apparent resistivity and phase inversions were relative errors of 0.05 and absolute errors of $0.02 \cdot 90/\pi \approx 0.6$ degrees, respectively, and for all geomagnetic data a low error floor of 0.01 was applied.

The RMS of the models shown below corresponds to the data misfit χ_d^2 from equation 6.6, divided by the total number N of data and taken the root of it. Internally, data of apparent resistivities are $\log_{10}(\rho)$, and therefore their corresponding errors are $\Delta\rho/(\rho \cdot \ln 10)$ (Gaussian error propagation). Note that the chosen error floors have *significant* influence on the final RMS if the data are not truly 2-D and/or the errors are *under*estimated by the processing. Therefore, if at least one of these two conditions is met, low error floors as chosen here
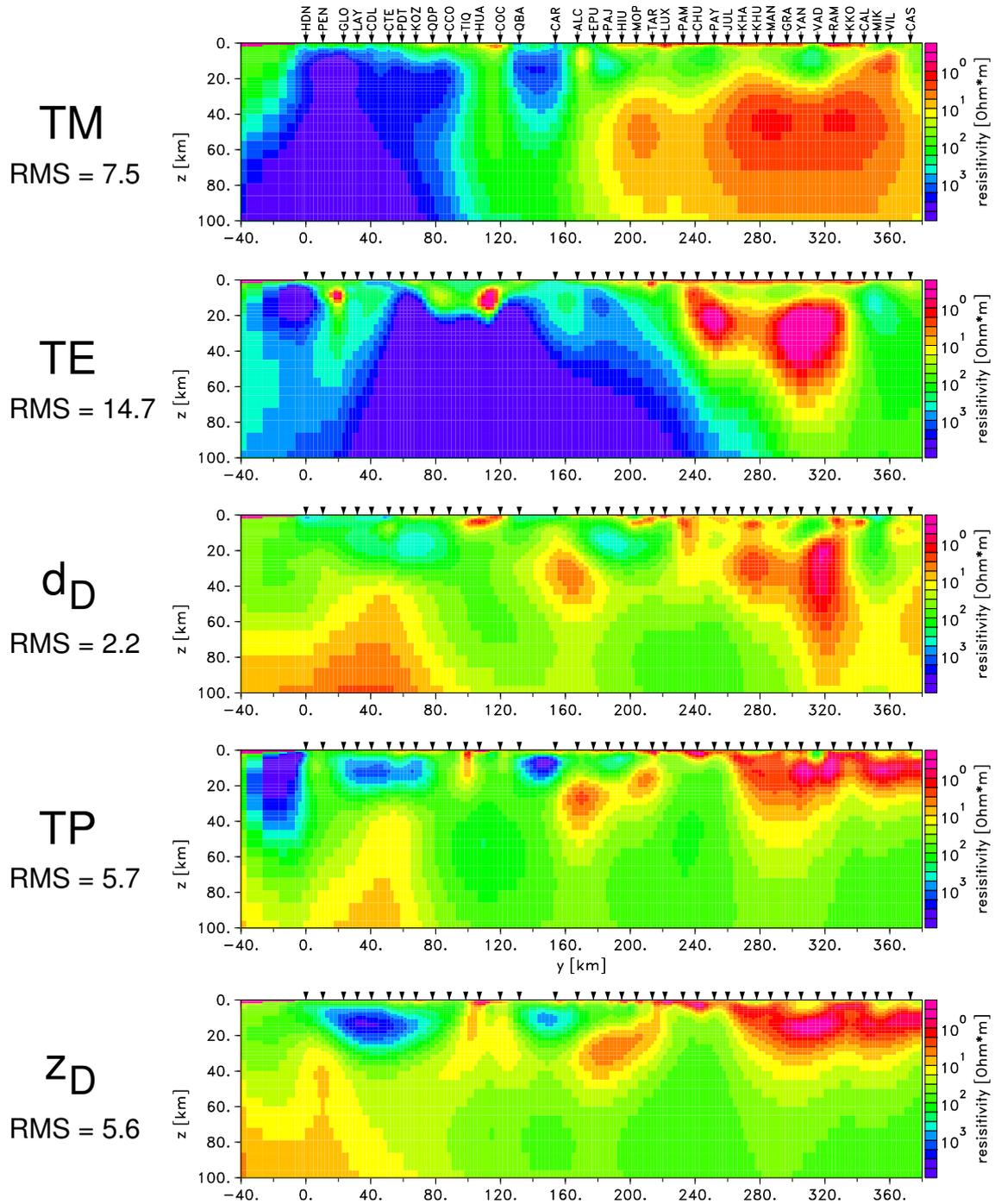
Figure 7.4: Inversion results for the ANCORP data, obtained from separate inversions of the five data types: apparent resistivities and phases of TM- and TE-polarization impedances, local induction vectors ('TP': real and imaginary parts of T_y), and the inter-station transfer functions d_D and z_D (real and imaginary parts of $B_y/B_y^0 - 1$ and B_z/B_y^0). For site – reference site grouping see table 7.1. For site locations see figure 3.2.

result naturally in a rather high RMS. For true 2-D data with pure Gaussian noise, an RMS of 1 is reasonable to be aspired, as this was also partly achieved in the synthetic modelling in section 6.

Though the resulting models are far from resembling each other, they all exhibit a highly conductive Precordillera anomaly and enhanced conductivities below the Altiplano. Inversion of TM-polarization data with a comparably acceptable data fit yields a smooth model with a resistive forearc, a rather superficial Precordillera anomaly and an Altiplano anomaly without indications of sharp boundaries. The TE-mode inversion model in contrast comprises sharp and very strong anomalies, which together with the high RMS and the disagreement with the TM-mode inversion demonstrates the higher dimensionality of this data, which, as mentioned, cannot partly be overcome by inclusion of small-scale heterogeneities in the 2-D modelling procedure as for the TM-mode. The choice of impedance eigenvalues instead of the original impedances obviously leads to the modelling of a small conductive anomaly between sites PEN and GLO in the Coastal Cordillera, which is exactly where the Atacama fault intersects the ANCORP profile. As eigenvalues cannot be regarded as undistorted two-dimensional data, and since all data types analyzed here have no signature of such anomaly, the dimensions of this structure cannot be investigated by 2-D modelling (see also section 5.1 and *Lezaeta* [2001]).

Compared to the results from impedance inversions, the forearc is not modelled resistive by geomagnetic transfer function inversions. In the Precordillera, these data types can all be adjusted by modelling a small-scale anomaly in very shallow depth, so that in view of accuracy, calculations including topography would be afforded. Forward modelling adjusting d_D and z_D as presented in *Soyer and Brasse* [2001] resolved the high conductive anomaly below the Precordillera extending between 3 km and 8 km depth. Also the strong anomalies in the Altiplano are in too shallow depth when compared with impedance inversions. Note that in all inversion models, but mostly in those from inversion of geomagnetic data, conductivities enhance particularly below the eastern part of the Altiplano. That this is required by magnetic data is visible to the naked eye from plots of induction vectors (figure 5.8) and perturbation vectors **q** (figure 5.9) at long periods: Zero B_z variation resp. maximal B_y variation at long periods is located near 67°W.

Models obtained from local tipper function (TP) and inter-station vertical to horizontal transfer function (z_D) inversions are highly similar. This might not be surprising since in both data types the local vertical magnetic field B_z is in the nominator and a magnetic east component in the denominator. However, at least for the author it is indeed astonishing, since on the one hand, the data result from very different analyses (TP: local bivariate, z_D: multivariate array analysis), and on the other hand due to the strong variation of B_y (reflected in d_D), these data are actually rather differing in terms of amplitude and gradient. Since a low error floor was applied, the RMS' of 5.6 and 5.7 reflect relatively good data fit. Yet, this does not imply that the inversions yield the 'right model': On most part of the eastern Altiplano, the resistivity-depth function of the two models with increasing depth yields the scheme: resistive–conductive–resistive, whereas observed apparent resistivities clearly comprise the scheme: conductive–resistive–conductive. Thus, these geomagnetic inversion results unfortunately mainly reflect 'just' the lateral variation of conductivities, what transfer functions involving the vertical magnetic field component are known to be most sensitive for. Inversion

of horizontal inter-station transfer functions d_D achieved by far the best data fit and places the Altiplano anomaly to slightly greater depths. It is however clear that the potential of a d_D inversion cannot be fully exploited in this study due to the lack of *one* common reference station.

Data have been further investigated by joint inversions of several data types, and three of the corresponding results are presented in figure 7.5. In all inversions involving impedance data, the error floor of apparent resistivities was set to a relative error of 0.1 and that of the phases again to $0.02\cdot90/\pi$. Geomagnetic data error floors were 0.01 throughout. Representer basis for calculation of the sensitivity matrix was the data subset of every second period at every second station (scheme 'checker', see *Siripunvaraporn and Egbert* [2000]). Data and responses of the three models at representative sites are shown in appendix B.

Joint inversion of the two inter-station data types d_D and z_D converged to a low RMS, and the similarity to the separate inversions of the two data types again reflects the high consistency of all geomagnetic data analyzed here. The uppermost structures on the Altiplano are in slightly higher agreement with impedance inversions than results from separate inversions of single geomagnetic data types.

Inversion of the two impedance polarizations yielded a model which is in general accordance with that presented by *Schwalenberg* [2000], with the main difference that here a lower boundary of the conductive structure below the Altiplano is indicated. The overall misfit resulted to 8.4, with better fit for the TM-mode data. Here, highest conductivities are observed in the central Altiplano, which is in contrast with the models from separate inversions of the two modes. It has been observed that an inversion of TE-mode impedances fails to converge since these data can obviously not be explained by 2-D modelling. Even downweighting of apparent resistivities with respect to the phases to account for static shift yields models which are in disagreement with geomagnetic data. Therefore, apparent resistivities of the TM-mode were jointly inverted together with geomagnetic data, and since these are all highly consistent and as it has been avoided to overweight data resulting from current flow along strike with respect to those of the other mode, only one geomagnetic transfer function, z_D, has been involved in this calculation. The resulting model now comprises highest conductivities in the eastern Altiplano, as demanded by magnetic data. Also, as already indicated in the separate inversion of the TM-polarization, a small moderately conductive anomaly between sites ALC and EPU is found, which is obviously an electrical image of active volcanism (volcano Olca is located close to the two sites). Note however that impedance data from these two sites are far from being 2-D (cf. regional strikes in figure 7.2). The Precordillera anomaly here consists of an upper and a lower part, as also deduced by *Lezaeta* [2001].
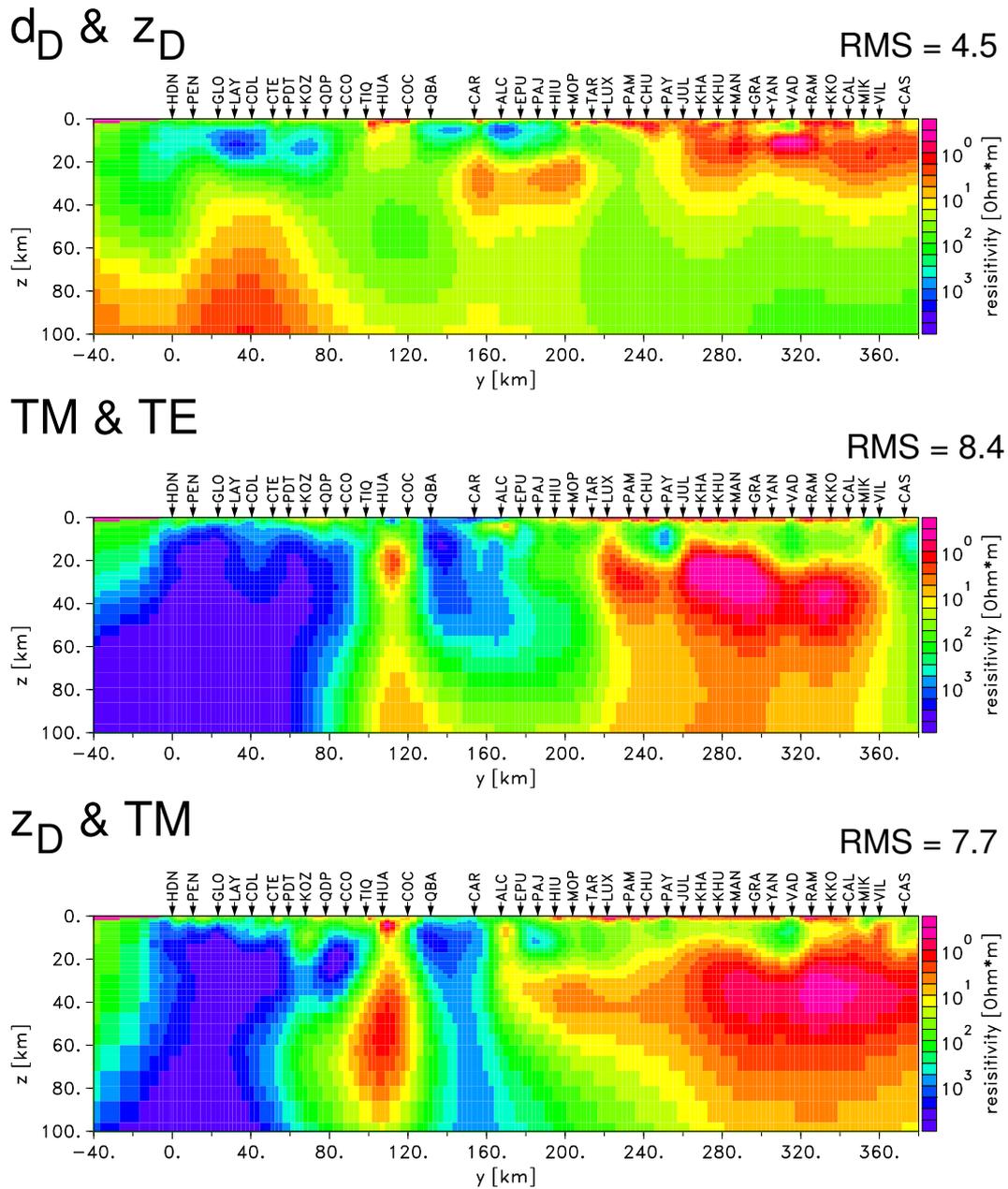
Figure 7.5: Joint inversion results for the ANCORP profile of inter-station geomagnetic data d_D & z_D, apparent resistivities and phases of TE- & TM-polarization impedances, and the impedance – geomagnetic transfer function combination TM & z_D. For site locations see figure 3.2.

7.4 Southern Andes

Dimensionality analysis of the impedance tensor has been performed by H. Brasse (see also *Brasse and Soyer* [2001]). Contour plots of the regional skew after *Bahr* [1988] for both profiles are shown in figure 7.6. Maximal skewnesses are observed in the Central Valley, partly exceeding the empirical threshold of 0.3, with generally higher values on the southern profile. Still, especially along the northern profile, skewness falls in the range [0–0.3], which encourages to model the data two-dimensionally.

Regional strikes were calculated after an approach by *Smith* [1997], which involves data of all periods (figure 7.7). Most strikes range between -5° and +5°, except for two stations in the Central Valley on the northern profile (where also high skewnesses are found), and several sites east of the volcanic chain on both profiles. The method also allows for calculation of a 'best' strike including data of all periods from all stations, which yielded strikes of N2°W for the northern and N1°E for the southern profile, respectively. Note that all strikes result from an analysis of unrotated impedances, i.e. tensors within a geomagnetic reference frame. Since average resp. 'best' strikes deviate insignificantly from zero, the structural strike is regarded as geomagnetic north, which is geographically ∼N9°E, and tensors were not rotated for 2-D modelling. This is also roughly consistent with the direction of the trench axis and the principal morphological strike onshore.

Besides the coast effect, induction vectors (fig. 5.8) at short periods mostly reflect small scale heterogeneities without significant strike direction: the anomalous regional strikes at stations DOY and PRA correspond to a rotation of local induction vectors in this area, and induction vectors at CVO clearly point away from Villarrica volcano. Induction arrows at longer periods, though being extremely uniform oriented, evince that the main morphological strike is not the only electromagnetic strike direction in the study area. As has been pointed out, the uniform north deflection is supposed to be on account of electrically anisotropic structures, embedded in a 2-D subsurface of differing strike direction. Geomagnetic perturbation data support this idea, since transfer functions h_H, d_H and h_D are very small and the spatial variation of d_D reflects the structural strike direction, as would be expected. Anisotropic 2-D modelling adjusting solely geomagnetic transfer functions is presented in section 8.
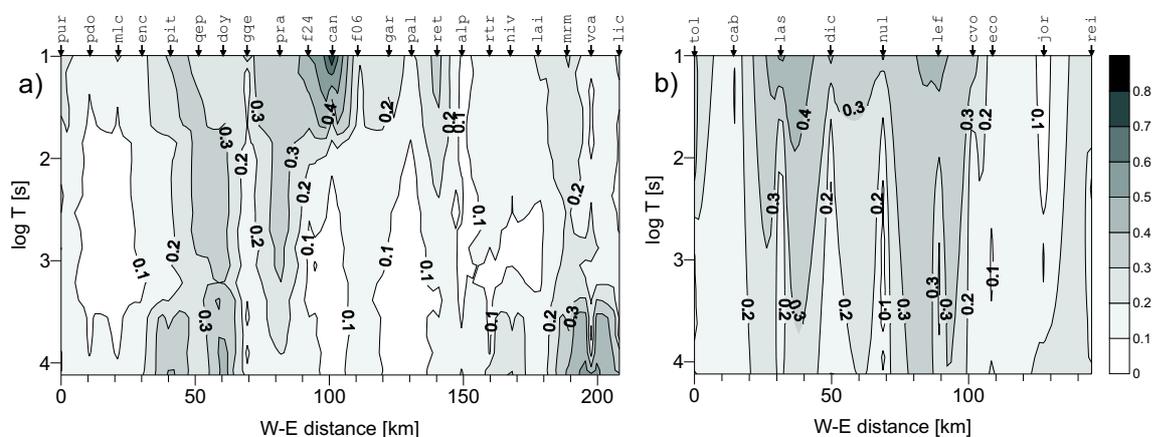
Figure 7.6: Contour plots of the regional skew after Bahr [1988] for the northern (left) and southern (right) profile (from Brasse and Soyer [2001]).
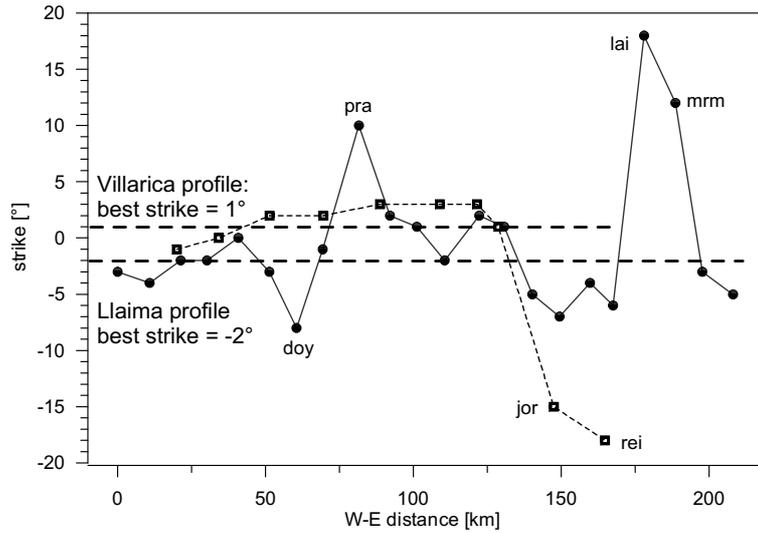
Figure 7.7: Regional impedance strikes for all sites of the two profiles, calculated after an approach of Smith [1997], which incorporates all periods. The best strikes result from a joint calculation for all periods and all sites of the corresponding profile (from Brasse and Soyer [2001]).

Though there is evidence for anisotropy, first investigation of impedance data was done by bimodal isotropic two-dimensional inversion as presented in *Brasse and Soyer* [2001] (figure 7.8). Again, apparent resistivities were downweighted with respect to the phases to account for static shift. The ocean was included as a conductive block in the start resp. a priori model. Both models comprise good conductors below and east of the volcanic arc resp. the Liquiñe-Ofqui fault in depth between 20 km and 40 km, with rather moderate conductivities (∼0.1 S/m) compared to anomalies from the Central Andes. Besides a good conductor in the Central Valley on the northern profile, the forearc is modelled resistive. This anomaly, which is also obtained if site PRA is omitted in the inversion, is clearly a 3-D effect since inversion at the southern profile does not yield such anomaly, and also induction arrows do not reflect such structure.

Plotting the two profiles onto a geological map which includes the major faults in that area, it is found that the western rim of the eastern conductive anomalies spatially coincides with the volcanic arc resp. Liquiñe-Ofqui fault, and the location of the observed 3-D structure in the Central Valley which is modelled here two-dimensionally is located at the intersection of the northern profile with the N40°W running Gastre fault zone, along which the volcanoes Villarrica, Quetrupillan and Lanin are aligned (figure 7.9, for site locations see figure 3.8).

As with data from the Central Andes, further investigation with isotropic 2-D inversion involves all available data types: apparent resistivities and phases of both polarizations (TE and TM), local induction vectors (TP) and the inter-station geomagnetic transfer functions d_D (horizontal to horizontal) and z_D (vertical to horizontal). Since all data were recorded within a single campaign and since one station (CAN, situated in the Central Valley) was deployed continuously for the whole era, data can all be referred to the same reference without construction of a synthetic array.
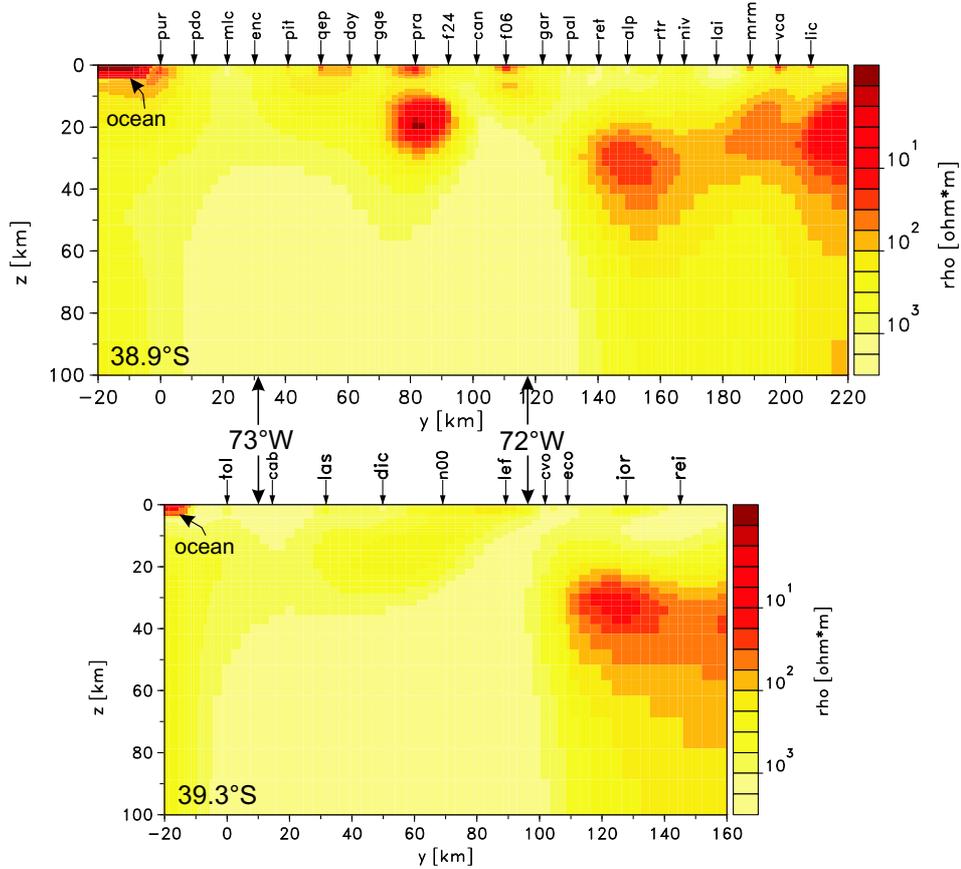
Figure 7.8: Results from bimodal apparent resistivity and phase inversions, as presented in Brasse and Soyer [2001].

Results from separate inversions of the data types are shown in figure 7.10 for the northern profile. Models are discretized by 158 columns and 51 rows plus 10 air layers for the TE-mode, and the ocean was again included in the start resp. a priori model and fixed during inversion, its base imaging roughly the true bathymetry with a sediment-filled trench of only 4 km depth. Apart from this structure, these models were homogeneous with a resistivity of 300 Ωm. Like before, representer basis for sensitivity matrix calculation was the data subset of every second period at all stations. Error floors in the impedance inversions were relative errors of 0.1 and 0.2 of apparent resistivities in the TM- and the TE-mode, respectively, and an absolute phase error of $0.02 \cdot 90/\pi$ for both modes. Minimum error for geomagnetic transfer functions was set to 0.01.

A short look at the inversion results makes clear that the TE-polarization data in the Central Valley are far from having 2-D signature, since the other inversion models do not exhibit such structure. Therefore, the anomaly modelled in *Brasse and Soyer* [2001] is only on account of the TE-mode data, and the missing of this structure in the southern profile even excludes an interpretation of this observation in terms of 2-D anisotropy, assuming the same structural strike as in the isotropic modelling. All inversion models exhibit lower resistivities to the east, with lowest values in the TM-polarization inversion (∼100 Ωm), where only a high RMS
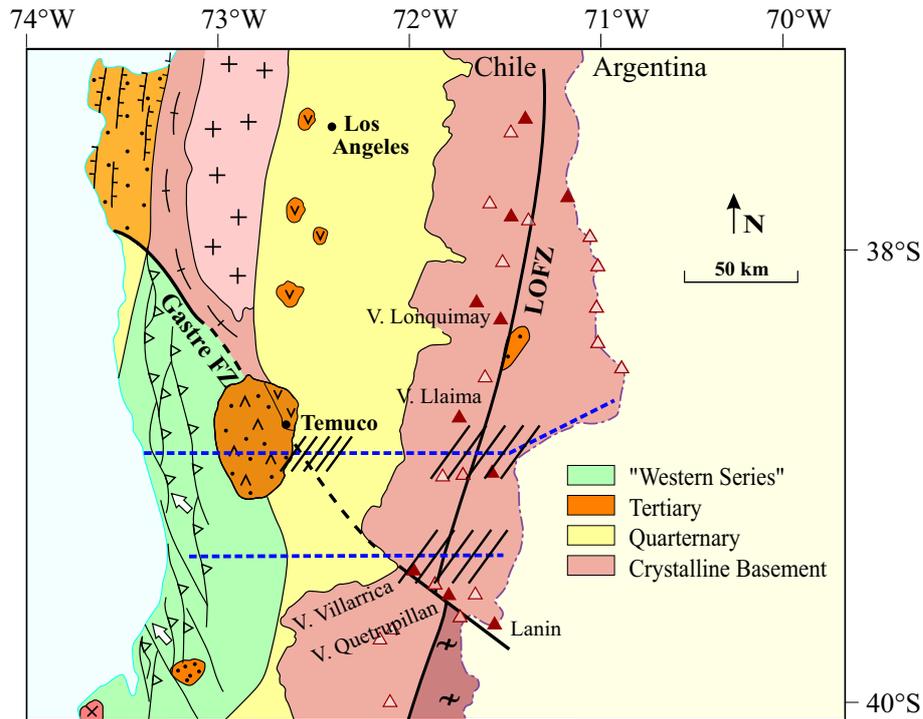
Figure 7.9: Geological map from H. Echtler (pers. comm.) for the southern study area showing the major fault zones (LOFZ: Liquiñe-Ofqui fault zone). The two dashed lines mark the profiles of this study, and hatched areas indicate the locations of conductivity anomalies as inferred by Brasse and Soyer [2001].

of 10.2 is achieved. Apart from the low resistivities below 40 km in the d_D inversion model, which is supposed to be on account of the proximity of the reference station to the anomalous conductivities, the models obtained by inversion of geomagnetic data are again of high consistency, and those which's data include B_z even resemble each other. Again, geomagnetic data are well fit by the inversion procedure.

Like for the northern study area, joint inversion of certain data types was performed for further investigation. Error floor of apparent resistivities in the TM-polarization was reduced to a relative error of 0.05, and all other minimum errors were set as before. The reduced basis for the sensitivity matrix calculation was a data subset of every second period at every second station (see *Siripunvaraporn and Egbert* [2000] for explanation). Results are shown in figure 7.11 and for a selected subset of stations, the data fit is presented in appendix B.

Inversion results for d_D and z_D again point out the high consistence within all geomagnetic data with respect to a two-dimensional model assumption. Note that this must also be the case for 2-D anisotropic conductivity distributions as discussed in section 8, since also in this environment, only currents along the structural strike have a vertical magnetic field component. Joint inversion of TE and TM polarization data yields a conductivity distribution which basically reflects the results presented in *Brasse and Soyer* [2001], as expected. Data of the TM-polarization inverted together with the inter-station transfer function z_D leads to small-scale structures, as required by the TM-polarization data, and compared to the single TM-mode inversion, slightly enhanced conductivities below the volcanic arc.
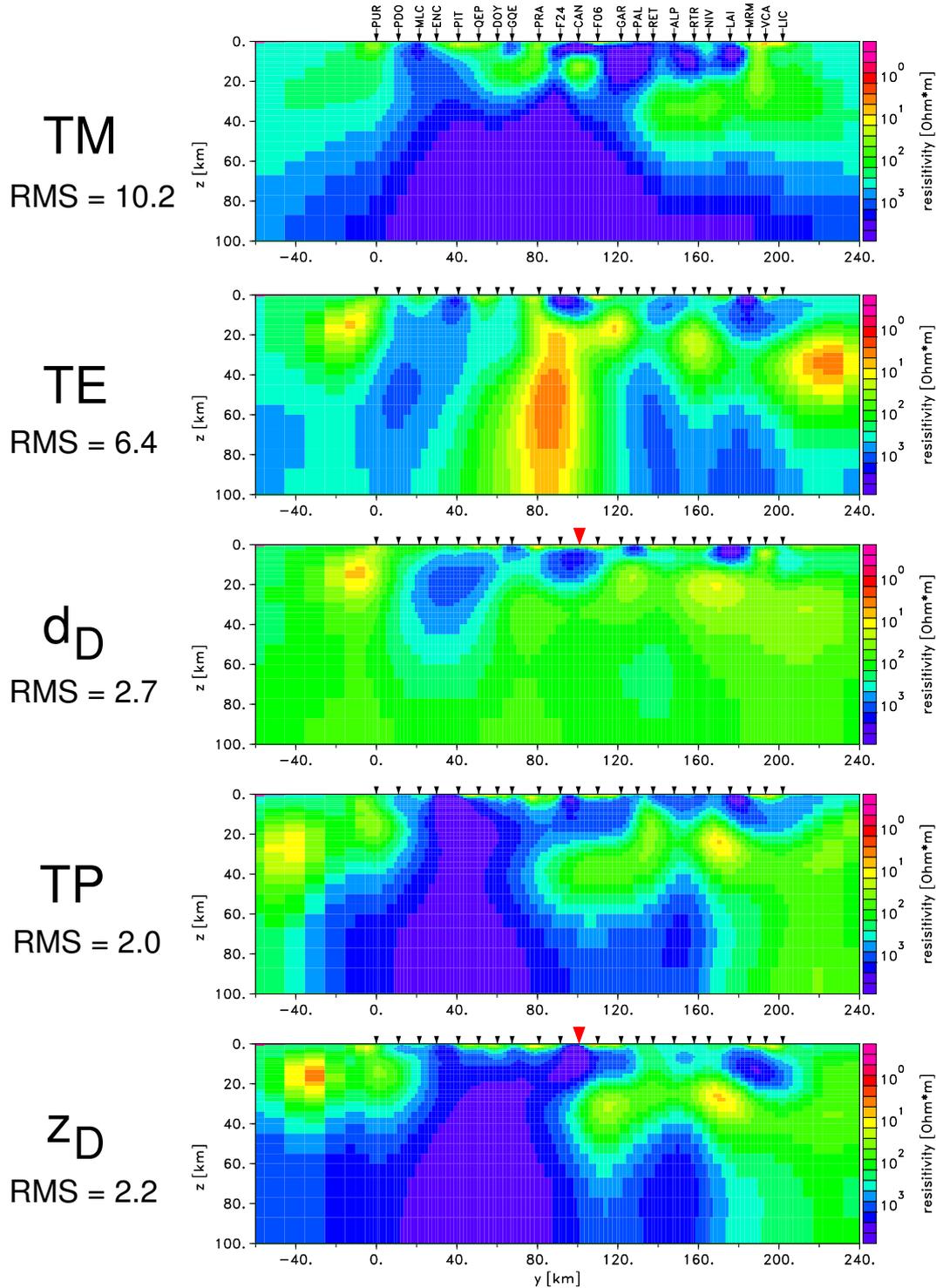
Figure 7.10: Inversion results for data of the northern profile in south Chile, obtained from separate inversions of the five data types: apparent resistivities and phases of TM- and TE-polarization impedances, local induction vectors ('TP': real and imaginary part of T_y), and the inter-station transfer functions d_D and z_D (real and imaginary parts of $B_y/B_y^0 - 1$ and B_z/B_y^0). Reference site is CAN, located in the Central Valley (red triangle). For site locations see figure 3.8.
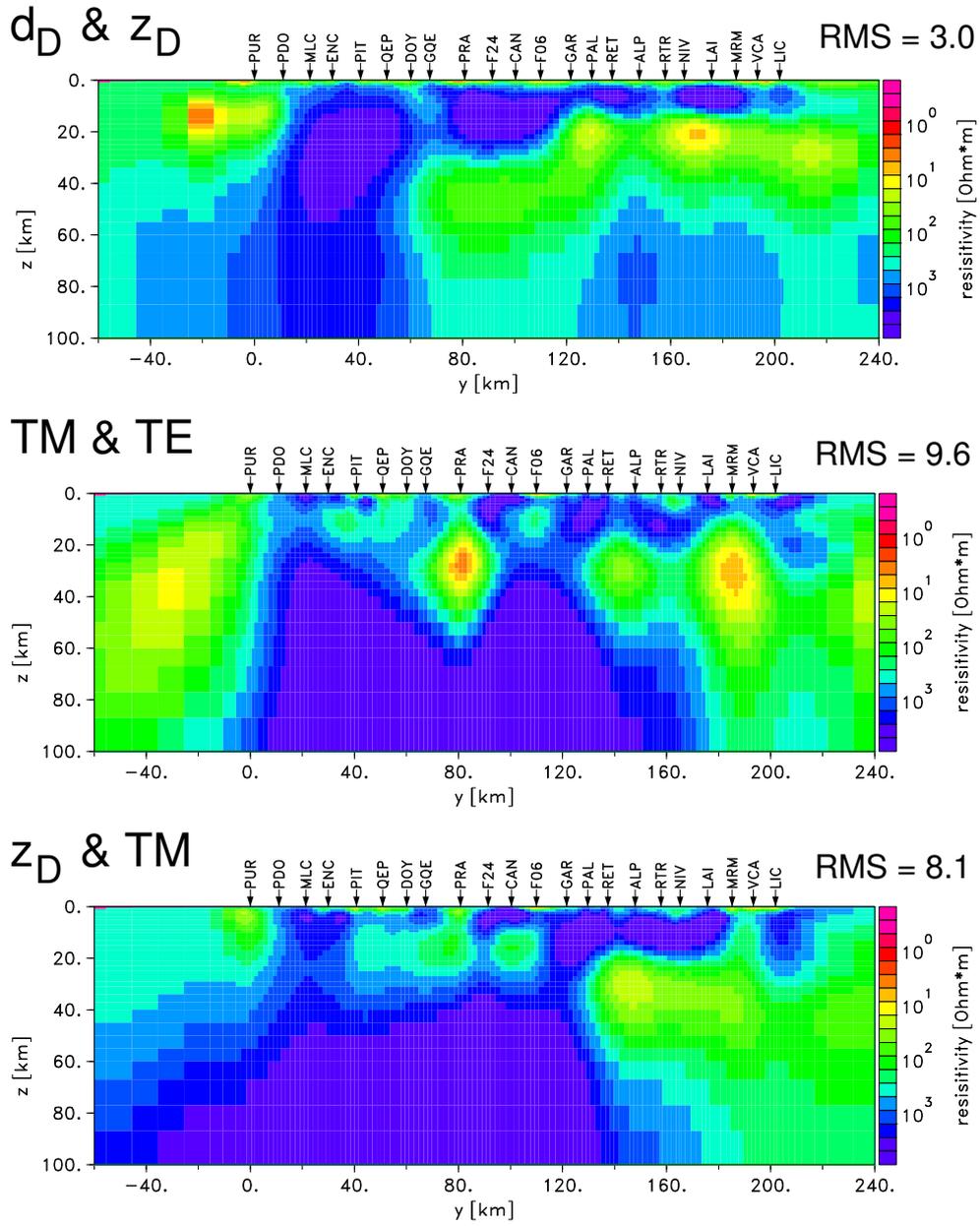
Figure 7.11: Joint inversion results for the northern profile of the south Chilean study area of inter-station geomagnetic data d_D & z_D, apparent resistivities and phases of TE- & TM-polarization impedances, and the impedance – geomagnetic transfer function combination TM & z_D. For site locations see figure 3.8.